Article

Selective Methanol Oxidation to Green Oxygenates—Catalyst Screening, Reaction Kinetics and Performance in Fixed-Bed and Membrane Reactors

Jan P. Walter [1,*], **Tanya Wolff** [2] **and Christof Hamel** [1]

[1] Institute of Process Engineering, Otto von Guericke University Magdeburg, Universitätsplatz 2, 39106 Magdeburg, Germany

[2] Max Planck Institute for Dynamics of Complex Technical Systems, Sandtorstraße 1, 39106 Magdeburg, Germany

[*] Correspondence: jan.walter@ovgu.de

Abstract: Experimental and simulation-based investigations are carried out for the selective oxidation of green methanol to the oxygenates dimethoxymethane (DMM) and methyl formate (MF), including an initial catalyst screening, the derivation of a reaction kinetic model, and a feasibility study of a fixed-bed and a membrane reactor with oxygen distribution. The catalyst screening of different supports and loading of vanadium revealed a 6.6 wt.-% VO_x/TiO_2 catalyst offering the highest potential to the formation for the target products. Kinetic experiments performed in a broad range of operation conditions, e.g., residence time, temperature, and oxygen concentration, are used for the postulation of a reaction network, providing the basis for mathematical modeling of the individual five reaction rates with a reduced mechanistic approach. A simulation study based on the derived reaction kinetics and parameters revealed the high potential of a distributed oxygen dosing at high residence times, outperforming the conventional fixed-bed reactor by up to 6% in the yield of DMM and up to 19% in the yield of MF. The formation of DMM is favored at low temperatures, whereas the formation of MF is supported by high temperatures.

Keywords: selective methanol oxidation; green oxygenates; solid acid/base catalysts; reaction kinetics; membrane reactors

1. Introduction

In order to limit global warming to 1.5 °C compared to preindustrial levels, a significant decrease in the consumption of fossil fuels is mandatory. To reduce the consumption of fossil resources in the chemistry industry and transportation sector, renewable energy can be applied for electrolytic hydrogen production, CO_2 capturing, and subsequent power-to-X processes [1,2]. Consequently, green feedstocks and sustainably produced intermediates, e.g., methanol (MeOH), can be used as CO_2 sinks [3] and subsequently converted into valuable green target products [4–7]. Numerous industrial-relevant chemicals, such as the green oxygenates dimethoxymethane (DMM) and methyl formate (MF), can be formed by the conversion of green MeOH [8–14]. The oxygenates, DMM and MF, are applied as fuel additives, green solvents, and raw material for further products [5,8,15–22]. Current production routes of DMM require two consecutive and locally separated steps, the initial formation of formaldehyde via dehydrogenation of MeOH in the gaseous phase and the following acetalization of MeOH and FA to DMM in the liquid phase [14,23,24]. The synthesis of MF is based on a homogeneously catalyzed equilibrium reaction of MeOH and carbon monoxide at pressures up to 45 bar [25–28]. Disadvantages such as apparative effort, corrosion, catalyst stability, and product separation within these processes lead to a need for alternative production routes [23,24,26,28]. An alternative to the state-of-the-art processes can be the direct selective oxidation of MeOH via bifunctional catalysts, as

can be recognized in Figure 1, forming both target products DMM and MF at the same catalyst surface and in one apparatus [29]. Due to the bifunctionality of the catalysts, a strong dependency between catalyst properties, reaction conditions, and product spectra results [14]. An excess of acidic sites shifts the product range to dimethyl ether (DME) since no previous oxidation step is required, whereas an excess of redox sites leads to the formation of deeper oxidation products such as formic acid (FAc), carbon monoxide (CO), and carbon dioxide (CO_2) [30].
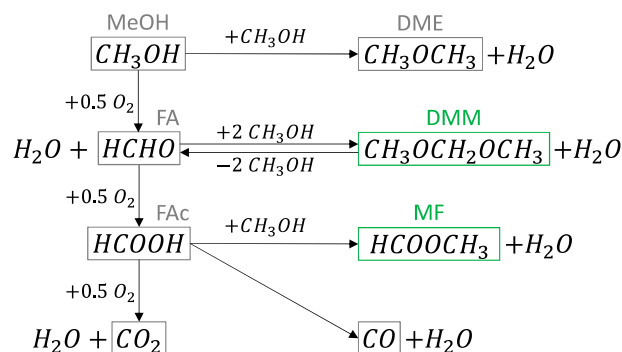
Figure 1. Reaction network of the selective oxidation of MeOH according to [12].

A lot of research has been conducted to figure out suitable bifunctional catalysts to increase the yield of DMM and MF as target products of the selective oxidation of MeOH [9,31–39]. VO_x-based catalysts show promising results within the formation of DMM and MF due to their high activity at low temperatures [19,24,29,31,38–40]. In addition, the aim of this study is a systematic investigation of the reaction conditions to figure out promising operation windows for the formation of DMM and MF on the reactor level in order to adjust temperature and local reactant concentrations to improve conversion and yields. In particular, the reaction temperature, residence time, and feed ratio between MeOH and oxygen (O_2) are considered. Initially, a catalyst screening is performed to figure out a suitable catalyst regarding the yield of DMM and MF. Additionally, a systematic experimental study of the influence of the reaction conditions on the conversion and selectivity behavior on the catalyst level is carried out. On this basis, the reaction network is refined by a reduction of the observed components and significant reactions within this study. The adapted reaction network is modeled by applying and parametrizing a kinetic description based on a reduced mechanistic approach. Finally, the derived and parametrized kinetic model is used to evaluate the potential of distributed dosing of O_2 in a packed-bed membrane reactor (PBMR) in comparison to the co-feed mode in a conventional fixed-bed reactor (FBR) by 1D simulation studies.

2. Results and Discussion

In the following section, the experimental results are shown. The catalyst screening is discussed first in Section 2.1.1 to figure out a suitable catalyst for the studied reaction network of the selective oxidation of MeOH. Based on this decision, kinetic experiments with the chosen catalyst are performed and discussed in Section 2.1.2 as a fundament for the mathematical modeling and simulation studies carried out and described in Section 2.2. The materials and methods used for the experimental and modeling part are explained in Section 3.

2.1. Experimental

2.1.1. Catalyst Screening

To evaluate the activity and the performance of catalysts with different compositions of supporting material and vanadium dotation, a catalyst screening is carried out. Six candidates have been tested, consisting of vanadium oxide on different supporting materials (γ-Al_2O_3, SiO_2, TiO_2) considered in the literature [19,30,39]. Two different vanadium load-

ings were tested individually for each supporting material. A detailed description of the catalyst preparation and structure-activity relations can be found in [41]. A temperature range between T = 100 °C and 300 °C, a weight hourly space velocity (WHSV = mass of catalyst/total volumetric flow rate) of WHSV = $1000 \, \text{kg} \cdot \text{s} \cdot \text{m}^{-3}$, and a feed ratio of MeOH and O_2 of $x^{in}_{MeOH} / x^{in}_{O_2} = 1$ are chosen initially for the first activity tests performed for the catalyst screening in this study. The feed concentration of MeOH is set to ($x^{in}_{MeOH} = 3$ vol.-%) in all experiments. More details regarding the experimental procedure can be found in Section 3.2. In Figure 2, the temperature dependencies of the yield of DMM (Figure 2a) and MF (Figure 2b) are shown. Figure 2 represents the selected samples of each tested supporting material. The conversion of MeOH, the selectivity of all occurring products, and the maximum reached yield of DMM and MF, respectively, are summarized in Table 1a,b for all tested catalysts. The listed parameters are used as key performance indicators.
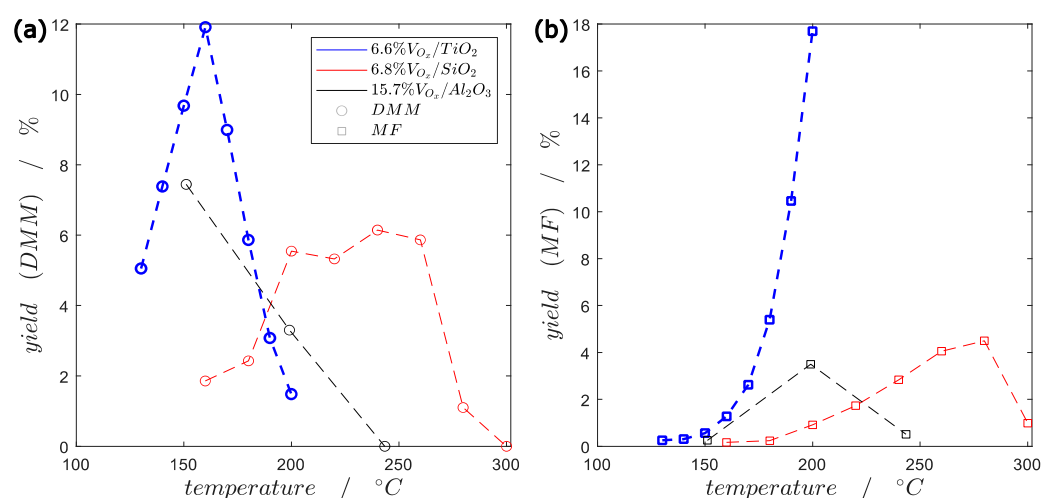
Figure 2. Temperature dependency of (**a**) the yield of DMM and (**b**) the yield of MF for 6.6 wt.-% VO_x/TiO_2, 6.8 wt.-% VO_x/SiO_2, 15.7 wt.-% VO_x/Al_2O_3; WHSV = $1000 \, \text{kg} \cdot \text{s} \cdot \text{m}^{-3}$, $x^{in}_{MeOH}/x^{in}_{O_2} = 1$.

Table 1. Conversion of MeOH, selectivity of all occurring products and maximum reached yield of (a) DMM and (b) MF for all tested catalysts; WHSV = $1000 \, \text{kg} \cdot \text{s} \cdot \text{m}^{-3}$, $x^{in}_{MeOH}/x^{in}_{O_2} = 1$.

(a)

Catalyst	Temperature [°C]	X(MeOH) [%]	S(DMM) [%]	S(MF) [%]	S(DME) [%]	S(FA) [%]	S(CO) [%]	Y_{max}(DMM) [%]
1.4%VO_x/Al_2O_3	150	16.4	26.3	16.5	57.2	0.0	0.0	4.3
15.7%VO_x/Al_2O_3	150	8.0	93.4	3.2	3.4	0.0	0.0	**7.5**
4.0%VO_x/TiO_2	200	15.9	24.5	12.4	5.6	57.5	0.0	3.9
6.6%VO_x/TiO_2	**160**	15.0	79.5	8.5	2.2	9.7	0.0	**11.9**
6.8%VO_x/SiO_2	240	25.1	24.4	11.3	4.9	59.4	0.0	**6.1**
15.9%VO_x/SiO_2	250	21.9	26.3	8.4	4.6	60.7	0.0	5.8

(b)

Catalyst	Temperature [°C]	X(MeOH) [%]	S(DMM) [%]	S(MF) [%]	S(DME) [%]	S(FA) [%]	S(CO) [%]	Y_{max}(MF) [%]
1.4%VO_x/Al_2O_3	150	16.4	26.3	16.5	57.2	0.0	0.0	2.7
15.7%VO_x/Al_2O_3	200	36.7	9.0	9.5	10.2	71.3	0.0	**3.5**
4.0%VO_x/TiO_2	250	67.8	0.6	8.5	2.9	83.7	4.3	5.8
6.6%VO_x/TiO_2	**200**	61.1	2.4	29.0	6.3	59.9	2.5	**17.7**
6.8%VO_x/SiO_2	280	80.3	1.4	5.6	3.0	87.8	2.2	**4.5**
15.9%VO_x/SiO_2	300	84.5	1.0	2.5	2.4	94.1	0.0	2.1

To choose the most promising candidate of all tested catalysts, the yield of DMM and MF are selected as decisive variables. As can be seen in Figure 2a,b, the highest yield of DMM and MF is reached with the 6.6 wt.-% VO_x/TiO_2 catalyst with a pronounced maximum for the yield of DMM at $T \approx 160\,°C$ and a continuously increasing yield of MF in the studied temperature range (up to $200\,°C$). Thus, this catalyst is chosen for further investigations regarding experimental and simulation-based studies, as described in the following sections. The important ratio of redox and acidic sites of this catalyst is 0.79, and additional properties can be found in [41,42].

2.1.2. Kinetic Experiments

To provide the basis for kinetic modeling in order to perform simulation studies, a suitable kinetic description of the reaction network is necessary. Therefore, experimental investigations are carried out systematically with the chosen model catalyst 6.6 wt.-% VO_x/TiO_2 in a broad range of operating conditions. The influences of residence time, the methanol-to-oxygen feed ratio ($x^{in}_{MeOH}/x^{in}_{O_2}$), and the impact of the temperature are studied ($T = 130–200\,°C$ with a step size of 10 K). In summary, 93 kinetic experiments are conducted.
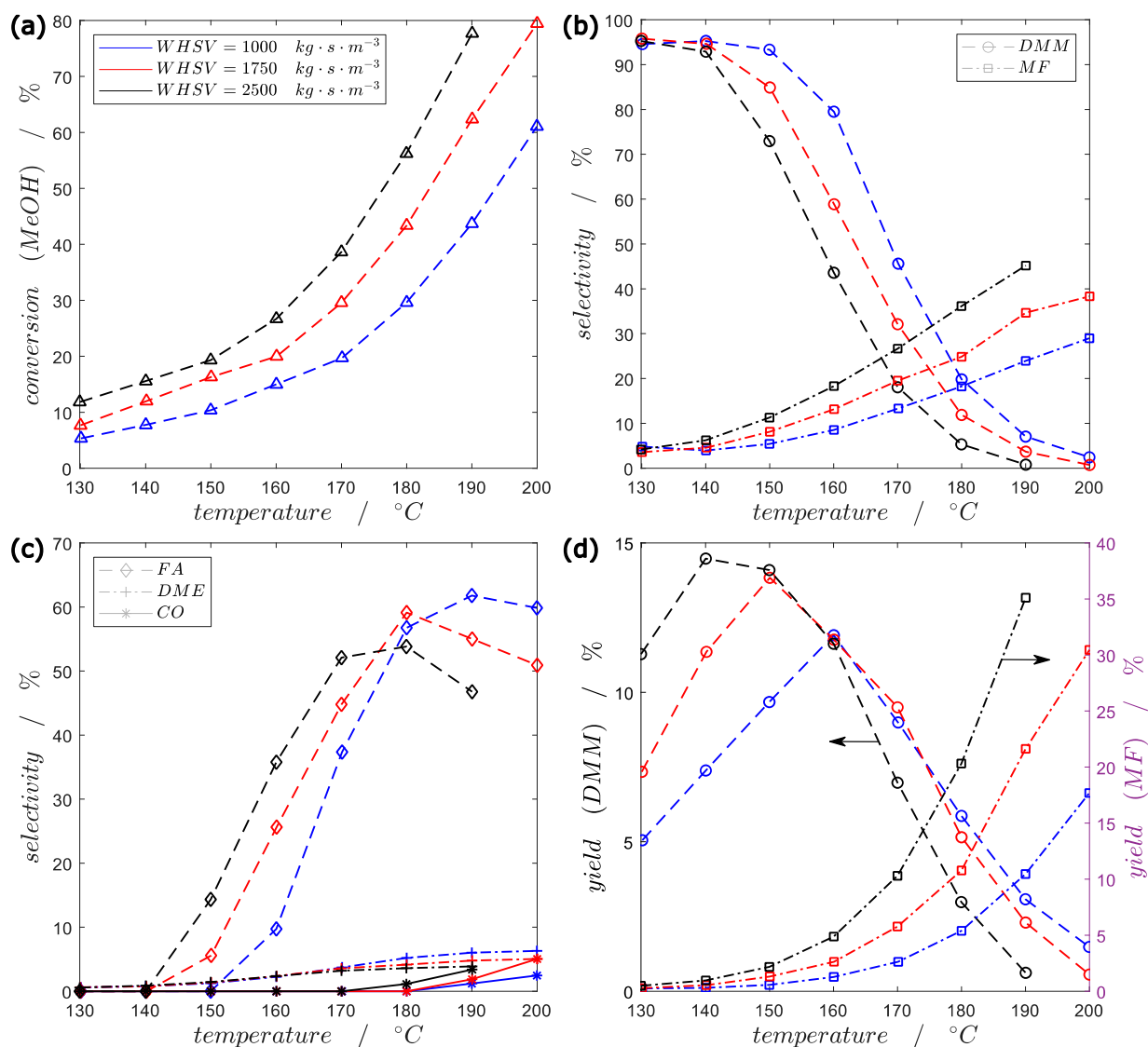
Influence of Residence Time

To study the influence of the residence time, the WHSV was varied between 1000, 1750, and $2500\,kg \cdot s \cdot m^{-3}$. The methanol-to-oxygen feed ratio remained constant at $x^{in}_{MeOH}/x^{in}_{O_2} = 1$, with $x^{in}_{MeOH} = 3$ vol.-%. The influence of the residence time and temperature on the key performance indicators is shown in Figure 3.

As can be seen in Figure 3a, the conversion of MeOH increases with higher residence times (WHSV) and temperature. Furthermore, it can be recognized in Figure 3b that the selectivity of DMM and MF is also strongly dependent on the residence time and the temperature. At conditions of low conversion of MeOH, the selectivity of DMM is high due to the high availability of MeOH, since three molecules of MeOH are necessary for the formation of DMM (see Figure 1). One molecule is required for the formation of FA by the oxidative dehydrogenation of MeOH. Two more molecules of MeOH are consumed in the consecutive acetalization with FA to DMM. These two contradictory effects, increasing conversion of MeOH and decreasing selectivity of DMM with increasing temperature, result in a maximum yield of DMM, as can be seen in Figure 3d. The maximum yield of DMM decreases and shifts to higher temperatures with a decreasing residence time. In contrast, the selectivity and yield of MF increase over the whole studied temperature range (see Figure 3b,d) with significant growth at $T \geq 150\,°C$. Lower than $T < 150\,°C$ DMM is the main favored product. Thus, the studied catalyst allows switching between the production of DMM and MF as a function of temperature. Additionally, it can be observed in Figure 3c that the residence time has a relevant influence on the formation of by-products (FA, DME, CO). The formation of FA is supported by $T < 170\,°C$ and high residence times, whereas $T \geq 170\,°C$ and high residence times favor the formation of CO, which can be depressed by low residence times. The selectivity of DME increases with temperature and a decreasing residence time since more unconsumed MeOH is available for the acidic-catalyzed formation of DME [24].
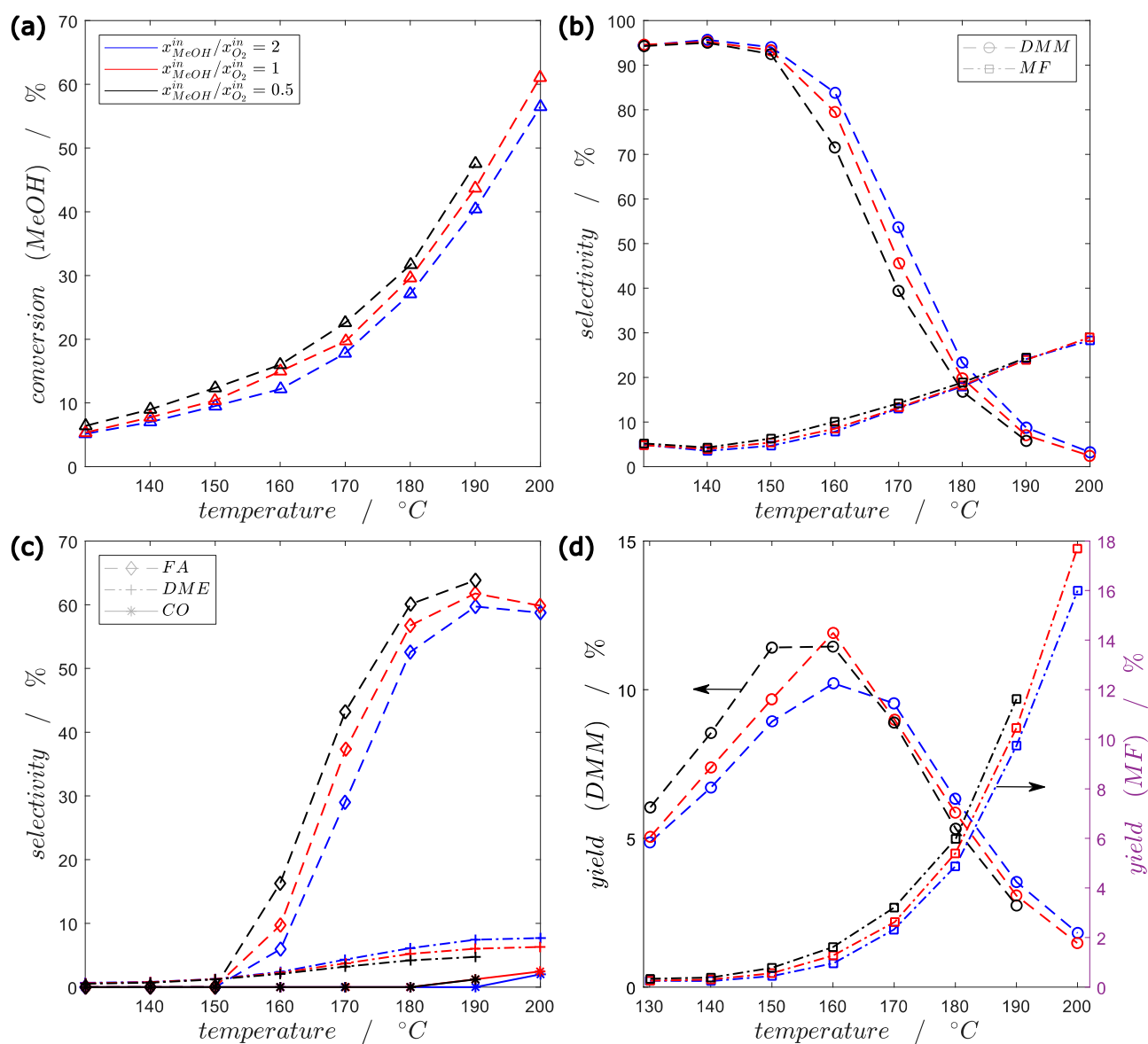
Influence of Oxygen Concentration

The influence of the concentration of O_2 is evaluated by a variation of the methanol-to-oxygen feed ratio of $x^{in}_{MeOH}/x^{in}_{O_2} = 0.25, 0.5,\ 1,\ 2$, whereas the feed concentration of MeOH and the residence time have remained constant ($x^{in}_{MeOH} = 3$ vol.-%; WHSV $= 1000\,kg \cdot s \cdot m^{-3}$). The impact of the concentration of O_2 on the key performance indicators is shown in Figure 4.

Figure 3. Influence of residence time and temperature on (**a**) conversion of MeOH, (**b**) selectivity of DMM and MF, (**c**) selectivity of FA, DME and CO, (**d**) yield of DMM and MF; $x^{in}_{MeOH}/x^{in}_{O_2} = 1$.

Figure 4a shows that the conversion of MeOH increases with an increasing concentration of O_2. An increasing concentration of O_2 also leads to a decreasing selectivity of DMM, depicted in Figure 4b. As already described in the sub-section before, the contradictory effects of increasing conversion of MeOH and decreasing selectivity of DMM with increasing temperature lead to a maximum in the yield of DMM. The maximum occurs at T = 160 °C for the given residence time, independent of the concentration of O_2, as shown in Figure 4d. An excess of O_2 is promising at T < 160 °C, whereas at T > 160 °C a shortage of O_2 is beneficial with respect to the yield of DMM since an excess of O_2 leads to a higher conversion of MeOH at lower temperatures and a shortage of O_2 to an improved selectivity of DMM at higher temperature (see Figure 4a,b). Figure 4b,c reveals that a higher concentration of O_2 leads to a significantly increased selectivity of FA and a slight increase in the selectivity of CO and the selectivity and yield of MF (Figure 4d).

In summary, kinetically dominated effects caused by the residence time, temperature, and the concentration of O_2 have to be considered with respect to the formation of the desired target products DMM and MF.

Figure 4. Influence of the concentration of O_2 and temperature on (**a**) conversion of MeOH, (**b**) selectivity of DMM and MF, (**c**) selectivity of FA, DME, and CO, (**d**) yield of DMM and MF; WHSV $= 1000 \, \text{kg} \cdot \text{s} \cdot \text{m}^{-3}$.

As described in the previous sections, both target products require contrary conditions to be favorably formed. At a higher residence time, temperature, and concentration of O_2, the reaction network shifts to FA and consecutively to MF, whereas at a lower residence time, temperature, and concentration of O_2, DMM is the major product. The yield of DMM is especially limited by a sharply decreasing selectivity with the increasing conversion of MeOH. To improve the yield of DMM, the kinetic coupling between the initial oxidative dehydrogenation of MeOH and the acetalization of FA and MeOH must be enhanced [43], e.g., by distributive dosing of O_2 via a membrane, which allows the control of the local residence time distribution, in particular, FA as a key intermediate in the reaction network. To figure out the potential of different dosing strategies influencing local concentrations of all species and residence time, first simulation studies are taken into account, analyzing the potential and reducing experimental efforts, respectively. Therefore, the reaction network has to be modeled mathematically by considering the influence of residence time, temperature, and concentration of O_2.

2.2. Reaction Kinetics and Reactor Concepts

In the following section, the results of the modeling part are shown. Initially, the derivation of reaction kinetics is described, followed by a feasibility study of different dosing concepts for MeOH and O_2 in conventional fixed-bed and membrane reactors to improve the yield of both target products on the reactor level.

2.2.1. Reaction Kinetics

Reaction Network Adaption

During the analysis of the kinetic experiments described in Section 2.1.2, not all components given in the reaction network presented by *Tatibouët* [12] (Figure 1) have been detected for the catalyst applied. Due to that reason, the reaction network is adapted (Figure 5) to the observed components and reactions in the studied operation window.
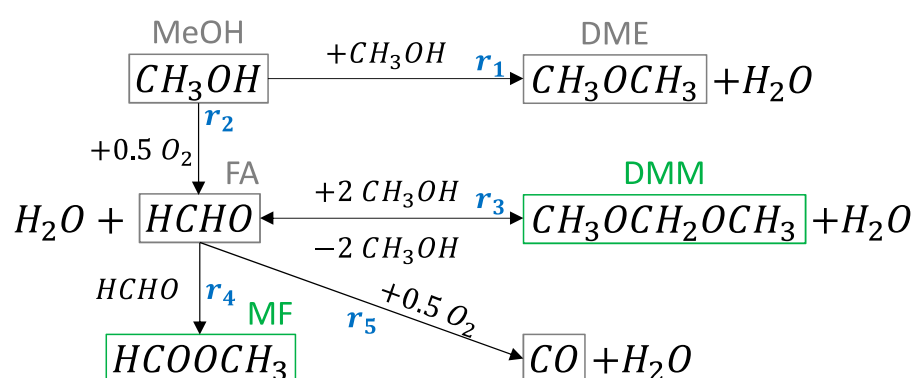
Figure 5. Adapted reaction network of the selective oxidation of MeOH.

The formations of FAc and CO_2 are removed since both products have not been detected within the analysis. Nevertheless, the consecutive reactions of FAc have to be considered due to the occurrence of MF and CO. According to *Broomhead* et al. [43], the formation of MF is described by a Tishchenko reaction of two molecules of FA (r_4). The formation of CO results in partial oxidation of FA (r_5), as considered by *Deshmukh* et al. [44] (r_5).

Consequently, the reaction network is reduced from nine to seven components and from seven to five reactions taking place (compare Figures 1 and 5). The adapted reaction network is the basis for the mathematical modeling and parameter estimation, described in the following sub-section.

Parameter Estimation

The reaction rates within the adapted reaction network (Figure 5) are derived from advanced rate expressions, considering adsorption effects and reaction equilibria [43,44]. Subsequently, the advanced rate expressions were fitted to the experiments conducted with the 6.6 wt.-% VO_x/TiO_2 catalyst and consecutively reduced to the following model by cutting out non-significant parameters:

$$r_1 = k_1 \cdot (p_{MeOH})^2 \tag{1}$$

$$r_2 = k_2 \cdot \frac{p_{MeOH} \cdot (K_{O_2} \cdot p_{O_2})^{0.5}}{(1 + K_{MeOH} \cdot p_{MeOH}) \cdot (1 + (K_{O_2} \cdot p_{O_2})^{0.5})} \tag{2}$$

$$r_3 = k_3 \cdot \left((p_{MeOH})^2 \cdot p_{FA} - \frac{p_{DMM} \cdot p_{H_2O}}{K_{3,eq}} \right) \tag{3}$$

$$r_4 = k_4 \cdot p_{FA} \tag{4}$$

$$r_5 = k_5 \cdot \frac{p_{FA} \cdot \left(K_{O_2} \cdot p_{O_2} \right)^{0.5}}{\left(1 + K_{MeOH} \cdot p_{MeOH}\right) \cdot \left(1 + \left(K_{O_2} \cdot p_{O_2}\right)^{0.5}\right)} \tag{5}$$

The temperature dependency of the reaction rate constants (k_j) is considered by the Arrhenius approach:

$$k_j = k_{j,0} \cdot \exp\left(-\frac{E_{A,j}}{R \cdot T}\right) \tag{6}$$

The adsorption equilibrium constant of O_2 is calculated as follows [45]:

$$K_{O_2} = K_{O_2,0} \cdot \exp\left(\frac{E_{ads,O_2}}{R \cdot T}\right) \tag{7}$$

The equilibrium constant of r_3 is calculated as follows:

$$K_{3,eq} = \exp\left(-\frac{\Delta H_{r,3}}{R \cdot T} + \frac{\Delta S_{r,3}}{R}\right) \tag{8}$$

The enthalpy of reaction ($\Delta H_{r,3}$) is calculated with the thermodynamical data of the gas phase reaction [46], whereas the entropy of reaction ($\Delta S_{r,3}$) is adjusted since the entropy decreases significantly if the reaction takes place at the catalyst surface instead of the gas phase [47].

The estimated parameters are summarized in Table 2 and show low confidence intervals. Mass transfer limitations can be neglected due to the Weisz-Prater criterion ($\Theta \approx 10^{-2}$) [48]. In Figure 6a–c, the parity plots of the yield of FA as an intermediate and key component of the reaction network and the yield of DMM and MF as target products are shown. The reduced model shows a good agreement with the experimental data obtained in this study. A comparison of experiments and simulations is depicted in Figure 6d for a varied WHSV, temperature, and a constant methanol-to-oxygen feed ratio of $x_{MeOH}^{in}/x_{O_2}^{in} = 1$. Figure 6d reveals the high predictability of the model with respect to the trends of the target product formation over the whole investigated temperature range, as can be seen exemplarily for the impact of the residence time.

Table 2. Estimated kinetic parameters for the reaction network of the selective methanol oxidation.

| Parameter	Value	Unit	Confidence Interval [%]
$k_{1,0}$	$6.84 \cdot 10^2$	$\mathrm{mol\,kg^{-1}s^{-1}\,Pa^{-2}}$	± 0.07
$k_{2,0}$	$9.98 \cdot 10^2$	$\mathrm{mol\,kg^{-1}s^{-1}\,Pa^{-1}}$	± 0.06
$k_{3,0}$	$7.89 \cdot 10^{-6}$	$\mathrm{mol\,kg^{-1}s^{-1}\,Pa^{-3}}$	± 4.50
$k_{4,0}$	$2.18 \cdot 10^{-2}$	$\mathrm{mol\,kg^{-1}s^{-1}\,Pa^{-1}}$	± 0.26
$k_{5,0}$	6.78	$\mathrm{mol\,kg^{-1}s^{-1}\,Pa^{-1}}$	± 0.09
$E_{A,1}$	128.51	$\mathrm{kJ\,mol^{-1}}$	± 0.02
$E_{A,2}$	80.78	$\mathrm{kJ\,mol^{-1}}$	± 0.05
$E_{A,3}$	25.70	$\mathrm{kJ\,mol^{-1}}$	± 0.03
$E_{A,4}$	47.00	$\mathrm{kJ\,mol^{-1}}$	± 0.04
$E_{A,5}$	71.46	$\mathrm{kJ\,mol^{-1}}$	± 0.05
$K_{O_2,0}$	14.97	$\mathrm{Pa^{-1}}$	± 0.04
E_{ads,O_2}	37.89	$\mathrm{kJ\,mol^{-1}}$	± 0.06
K_{MeOH}	$5.45 \cdot 10^{-4}$	$\mathrm{Pa^{-1}}$	± 2.54
$\Delta S_{r,3}$	0.26	$\mathrm{kJ\,mol^{-1}K^{-1}}$	± 0.10
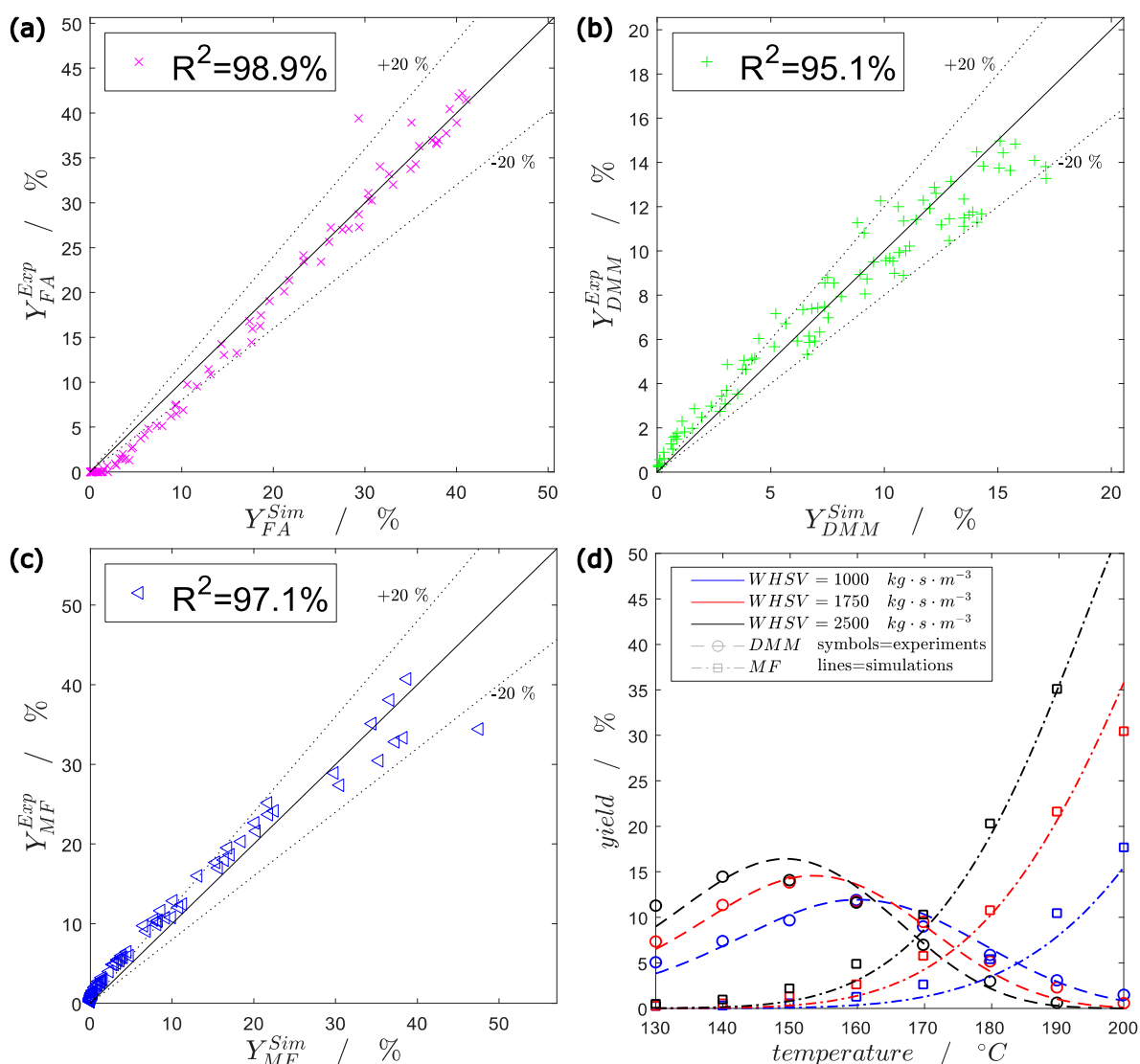
Figure 6. Parity plot of (**a**) the yield of FA, (**b**) the yield of DMM, (**c**) the yield of MF, (**d**) comparison of experimental and simulated data for a variation of WHSV and temperature ($x_{MeOH}^{in}/x_{O_2}^{in} = 1$).

2.2.2. Feasibility Study of Different Reactor Concepts and Dosing Strategies (FBR vs. PBMR)

To evaluate the potential of feeding reactants in a co-feed mode in an FBR and distributed dosing of O_2 in a PBMR simulation studies with a simplified 1D, isothermal, plug flow model are carried out (Equations (9) and (16), Section 3.3). The used tube-to-shell-side feed ratio in the PBMR, which influences the local residence time of all species involved, is set to 1/8, and the inlet concentrations of O_2 and MeOH to 21 vol.-% and 3 vol.-%, respectively, based on previous investigations [42,49–53]. In order to analyze suitable reaction conditions for the FBR and the PBMR, the residence time (WHSV) and the temperature are varied. The reactor concepts are compared with respect to the conversion of MeOH, the selectivity of FA, and the selectivity and yield of DMM and MF. The results are shown in Figure 7.
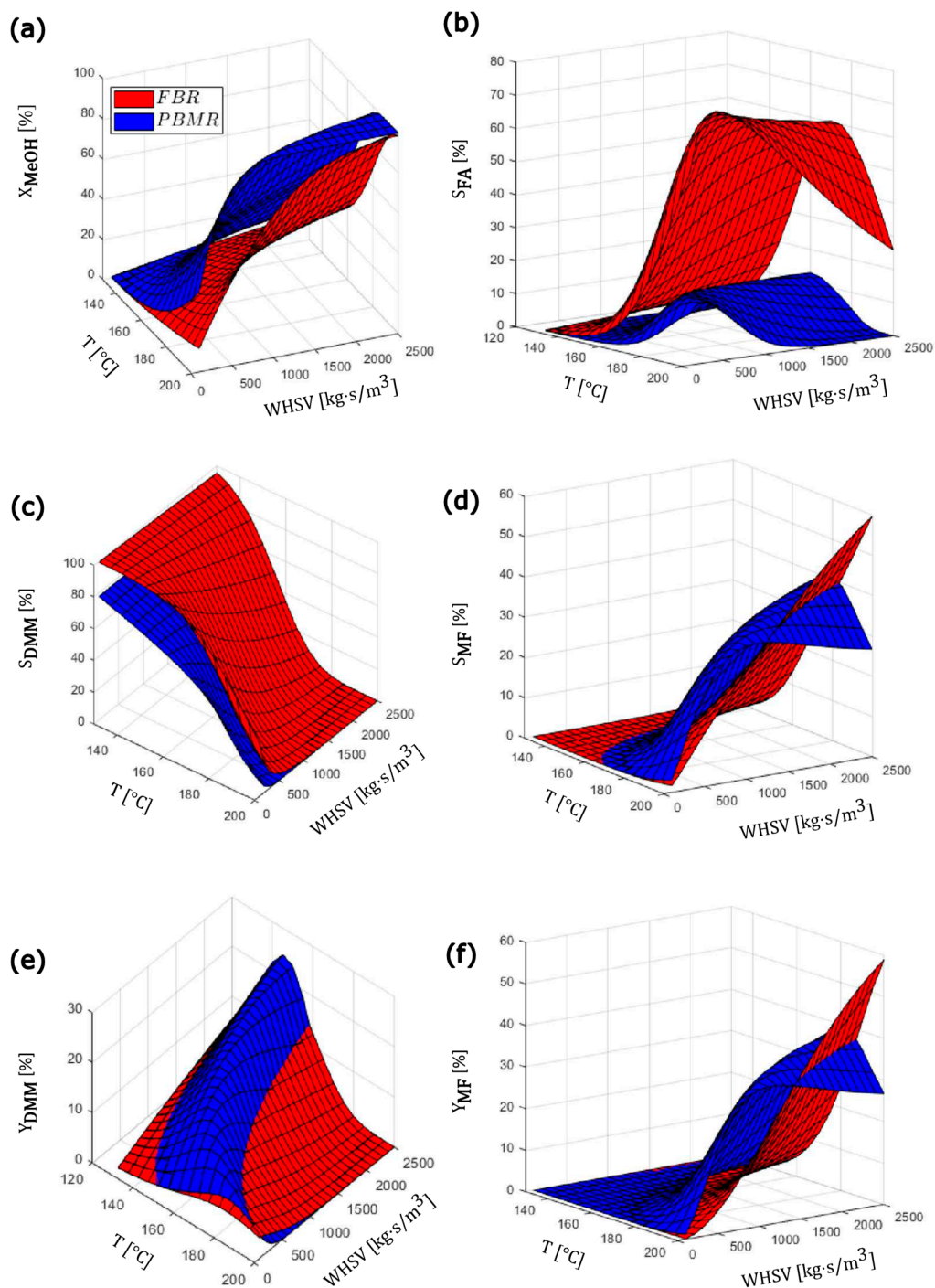
Figure 7. Comparison of FBR and PBMR: (**a**) conversion of MeOH, (**b**) selectivity of FA, (**c**) selectivity of DMM, (**d**) selectivity of MF, (**e**) yield of DMM, (**f**) yield of MF; $x_{O_2}^{in} = 0.21$.

As shown in Figure 7a, the conversion of MeOH can be significantly increased by a distributed dosing of O_2 in membrane reactors controlling the local residence time, independent of the total residence time and temperature. This effect results in higher local concentrations of MeOH in the PBMR and supports the formation of FA and DME. The initially formed FA leads to a higher selectivity of MF in the PBMR up to a temperature of 180 °C, which is why the selectivity of DMM is lowered compared to the FBR case (Figure 7c,d). However, between 140 and 180 °C, the increase in the conversion of MeOH dominates the decrease in the selectivity of DMM, leading to a significantly increased yield of DMM by dosed O_2 along the axial reactor coordinate (Figure 7e). As a result, the

maximum yield of DMM is more pronounced in the PBMR than in the FBR. Furthermore, Figure 7f reveals that the PBMR offers potential with respect to the formation of MF up to 180 °C due to the increased conversion of MeOH and the enhanced selectivity of MF caused by an improved kinetic coupling between the formation and the consecutive reaction of FA. The improved kinetic coupling is characterized by the lowered selectivity of FA and the increased selectivity of MF (Figure 7b,d).

In conclusion, a distributed dosing of O_2 via a PBMR by manipulating the local concentration of O_2 and residence time profiles offers the potential to improve the formation of DMM and MF due to better control of the initial formation of FA by the oxidative dehydrogenation of MeOH and the kinetic coupling between this initial step and the consecutive reaction steps to the target products.

3. Materials and Methods

In this section materials and methods, which are used for the experimental and model-based studies, are described.

3.1. Catalysts

Various catalysts were used consisting of VO_x on different supporting materials (Al_2O_3, SiO_2, TiO_2). The catalysts were prepared by wet impregnation with vanadyl acetylacetonate in acetone. The synthesis and a detailed characterization (BET, V-density, XRD, DRIFT spectra, V-NMR, TPR, TPD) of all catalysts tested within this study were done by *Klose* et al. in previous investigations. Additional information and corresponding figures can be found in [41].

3.2. Experimental

The catalytic activity was tested in a laboratory fixed-bed reactor. The overall plant design consists of the reactor of a saturation column filled with Raschig rings and MeOH used to transfer MeOH from the liquid phase into the gaseous reaction phase. Additionally, for the analysis, a gas chromatograph (GC) was installed (GC 6890 B, Agilent Technologies, Santa Clara, CA, USA). In front of the GC, a 16-port multi-position valve (VICI-Valco Instruments Co. Inc., Houston, TX, USA) is installed to enable samples of the feed gas and the product stream. The sample line between the reactor outlet and the GC, including the multi-position valve, is maintained at 150 °C to avoid condensation. The feed stream contains gasified MeOH (Honeywell International Inc., Charlotte, North Carolina, purity $\geq$ 99.9%), nitrogen (Linde plc, purity of 99.999%), and air (technical grade). The gas streams can be set via mass flow controllers (MFC) (EL-Flow, Bronkhorst High-Tech B.V., Ruurlo, The Netherlands).

The used fixed-bed reactor consists of a quartz glass tube with a length of 35 cm and an inner diameter of 6 mm. The catalyst material with a particle diameter of 1 mm was placed in the middle of the tube. A thermocouple was positioned in the center of the catalyst bed to measure the reaction temperature. The tube was placed in an electrical furnace for heating or cooling, respectively, to keep the reaction temperature constant (isothermal conditions). In the front and the back of the catalyst-bed, inert material (1.0 mm–1.25 mm 68 wt.-% ZrO_2, 32 wt.-% SiO_2, Mühlmeier GmbH & Co. KG, Bärnau, Germany) was filled into the tube to provide a heating or cooling zone, respectively. For all experiments, 1 g of catalyst was used. The different bulk densities of the catalysts tested differed in the lengths of the catalytic active zones. The length of the catalytic active zone of the 6.6 wt.-% VO_x/TiO_2 catalyst was 2.4 cm.

The GC was equipped with an HP-PLOT/Q column for the separation of CO_2, H_2O, FA, and FAc. DME, DMM, MF, and MeOH were separated by a DB-FFAP column and detected with a flame ionization detector (FID). The GC was additionally equipped with an HP-Molesieve 5 A column (Agilent Technologies, Santa Clara, CA, USA) to separate O_2, N_2, and CO. The HP-PLOT/Q and the HP-Molesieve 5 A column were related to a temperature conductivity detector (TCD) to detect the components.

The catalyst was pretreated for 2 h in an airflow of 50 mL/min at a temperature of 400 °C before each parameter set was tested to assure a fully oxidized state.

To study the impact of the residence time, three different values of WHSV were tested (1000, 1750, and 2500 kgs/m^3). The WHSV values were set at the ambient temperature in the laboratory (20 °C). Furthermore, the influences of O_2 and MeOH were tested by applying an excess of O_2 ($x^{in}_{MeOH}/x^{in}_{O_2}$ = 0.5 and 0.25), equality ($x^{in}_{MeOH}/x^{in}_{O_2}$ = 1), and a shortage of O_2 ($x^{in}_{MeOH}/x^{in}_{O_2}$ = 2) by adjusting the volumetric flow rates of MeOH, O_2, and N_2. The concentration of MeOH was set to 3 vol.-% in all experiments. The pressure drop across the reactor and the temperature in the saturator were held constant in all experiments at 0.1 bar and 20 °C, respectively, to assure equal saturation conditions of MeOH. Each set of parameters was held approximately for 4 h until all GC samples (two of the feed streams and three of the product stream) were analyzed.

3.3. Mathematical Modeling

3.3.1. Parameter Estimation

The experimentally-used FBR is modeled by applying a 1D mass balance equation, assuming steady-state, plug flow, ideal gas behavior, and isothermal and isobar conditions:

$$\frac{d\dot{n}_i}{dz} = \frac{m_{cat}}{L} \cdot \sum_{j=1}^{M} \nu_{i,j} \cdot r_j \tag{9}$$

The resulting system of ordinary differential equations (ODEs) is solved with the solver ode15s in Matlab$^{®}$. The objective function for parametrizing the reaction network given in Figure 5 is defined as follows:

$$OF = \sum_{k=1}^{N_{Exp}} \left(\lambda_k^{Sim} - \lambda_k^{Exp} \right)^2; \tag{10}$$

$$\lambda_k = [X_{MeOH}, S_{DMM}, Y_{DMM}, Y_{MF}, Y_{FA}, Y_{DME}, Y_{CO}] \tag{11}$$

The total number of kinetic experiments is N_{Exp} = 93. For the optimization, a Gauß-Newton algorithm with a trust region reflective approach is used, provided by the lsqnonlin function of Matlab$^{®}$. λ_k is a vector of the conversion of MeOH (X_{MeOH}), the selectivity (S_i), or the yield (Y_i) of component i, respectively, which are determined simulative (*Sim*) or experimentally (*Exp*):

$$X_{MeOH} = \frac{\dot{n}^{in}_{MeOH} - \dot{n}_{MeOH}(z = L)}{\dot{n}^{in}_{MeOH}}; \ S_i = \frac{\dot{n}_i(z = L) - \dot{n}^{in}_i}{\dot{n}^{in}_{MeOH} - \dot{n}_{MeOH}(z = L)} \cdot \frac{\left| \nu_{MeOH,j} \right|}{\nu_{i,j}}; \ Y_i = X_{MeOH} \cdot S_i \tag{12}$$

The molar flow rate of component i at the inlet of the reactor ($z = 0$) ($\dot{n}^{in}_i$) is calculated as follows:

$$\dot{n}^{in}_i = x^{in}_i \cdot \dot{n}, \text{ with} \tag{13}$$

$$\dot{n} = \frac{p \cdot \dot{V}}{R \cdot T} \text{ and} \tag{14}$$

$$\dot{V} = \frac{m_{cat}}{WHSV}. \tag{15}$$

x^{in}_i is the molar fraction at the inlet of the reactor, $\dot{n}$ is the total molar flow rate, and $\dot{V}$ is the total volumetric flow rate.

3.3.2. Simulation Studies of FBR and PBMR

To model the PBMR, an additional source term for the membrane flux (J_i) is added to the mass balance equation of the FBR (Equation (9)):

$$\frac{d\dot{n}_i}{dz} = \frac{m_{cat}}{L} \cdot \sum_{j=1}^{M} \nu_{i,j} \cdot r_j + J_i \tag{16}$$

$$J_i = \frac{\dot{n}_{i,ss}^{in}}{L}. \tag{17}$$

Both reactor concepts are comparable since the total molar flow rate at the outlet of both reactors ($z = L$) is identical in the absence of chemical reactions, as shown in Figure 8a. Therefore, the total molar flow rate of the PBMR is divided into two separate inlet flow rates, the inlet flow rate of the tube-side ($\dot{n}_{ts}^{in}$) and the inlet flow rate of the shell-side ($\dot{n}_{ss}^{in}$), by the tube-to-shell-side feed ratio (ts/ss), resulting in significantly higher local residence times in the PBMR (Figure 8b):

$$\dot{n}_{ts}^{in} = \dot{n} \cdot \left(1 - \frac{1}{1 + ts/ss}\right); \; \dot{n}_{ss}^{in} = \dot{n} \cdot \frac{1}{1 + ts/ss}. \tag{18}$$
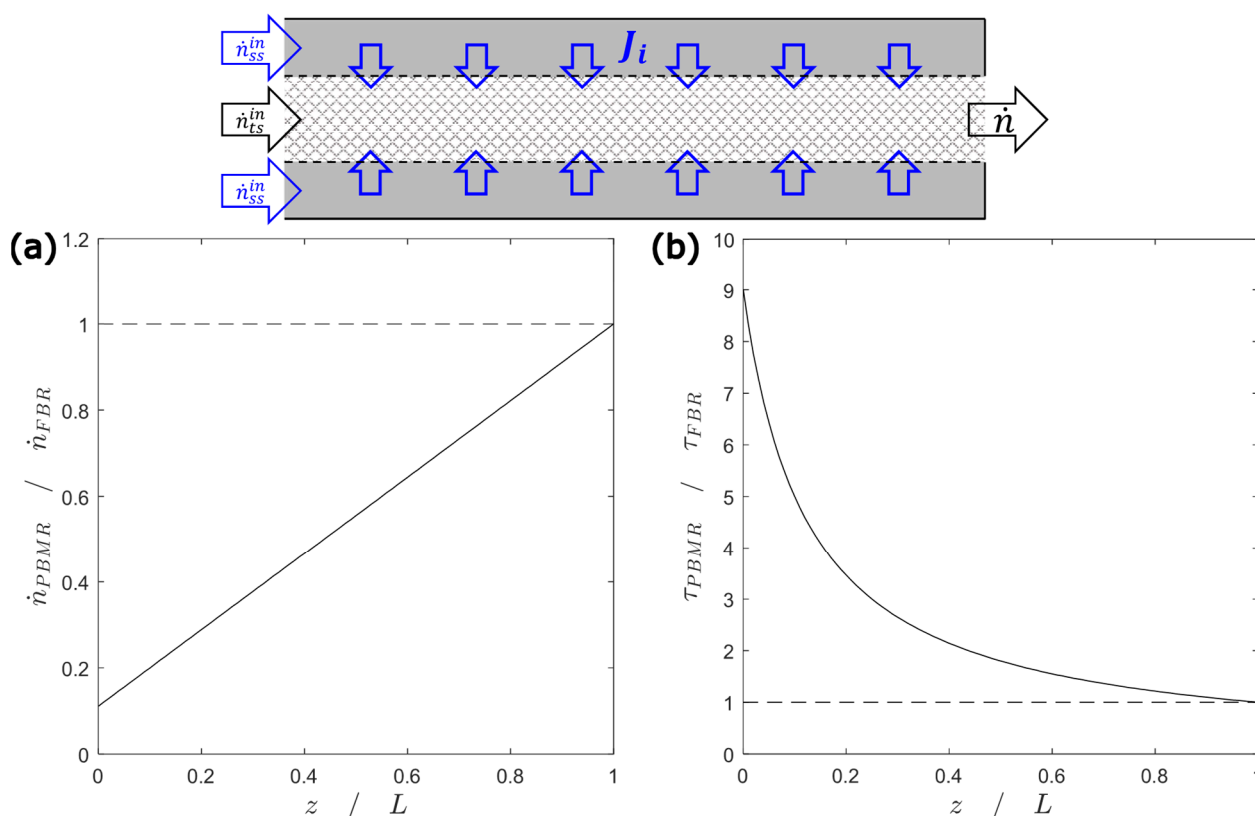
Figure 8. (**a**) Ratio between the local molar flow rate of the PBMR and the FBR, (**b**) Ratio between the local residence time of the PBMR and the FBR; ts/ss = 1/8.

4. Conclusions and Outlook

In this contribution, experimental and simulation-based investigations were carried out for the selective oxidation of green methanol (MeOH) to the oxygenates dimethoxymethane (DMM) and methyl formate (MF). Initially, a catalyst screening and preselection were conducted to figure out a promising catalyst for the formation of both target products. The catalyst screening was conducted at WHSV = $1000 \, \mathrm{kg \cdot s \cdot m^{-3}}$, $x_{MeOH}^{in}/x_{O_2}^{in} = 1$ and a temperature

range between T = 100 °C and 300 °C. The catalyst composition 6.6 wt.-% VO_x/TiO_2 offered the highest potential with a maximum yield of DMM of 11.9% and 17.7% for MF in the investigated operation window.

Additionally, 93 kinetic experiments with the chosen catalyst were performed to figure out the influence of the residence time, the temperature, and the methanol-to-oxygen feed ratio on the target product formation. The highest selectivity of DMM is reached at low residence times (WHSV = 1000 kgs/m^3) and oxygen (O_2) shortage $x_{MeOH}^{in}/x_{O_2}^{in} = 2$, whereas the yield of DMM is supported by high residence times and oxygen excess due to increased conversion of MeOH. Temperatures up to 160 °C are favorable for the formation of DMM. In contrast, the yield of MF increases with enhanced temperature, increasing concentrations of O_2, and residence times, respectively. The impact of the residence time and temperature on the reaction network is more pronounced than the influence of the concentration of O_2.

Based on the kinetic experiments, the reaction network given in the literature was adapted to the observed reactions and components in this study. The reaction network was reduced from seven to five reactions and from nine to seven components. The reaction rates were described mathematically with a reduced and adjusted mechanistic model and corresponding reaction kinetic parameters were estimated. With the derived mathematical model, a good agreement between experimental and simulated results and a high predictability of trends for the formation of the target products was achieved.

The model was finally used to investigate the potential of distributive dosing of O_2 in a packed-bed membrane reactor (PBMR), influencing the local concentration of O_2 and residence time profiles in comparison to the co-feed mode of a conventional fixed-bed reactor (FBR). The simulation study revealed that high residence times are beneficial for the formation of both target products, independent of the reactor and dosing concept. The formation of both target products can be enhanced by the distributive dosing of O_2 via a membrane. The yield of DMM can be improved at low temperatures ($\Delta Y(DMM) \approx 6\%$) due to a higher conversion of MeOH, whereas the selectivity and, thus, the yield of MF is significantly enhanced up to 180 °C ($\Delta Y(MF) \approx 19\%$). Obviously, the simulation study performed offered potential for a distributed dosing of oxygen in membrane reactors for the selective oxidation of methanol to platform chemicals MF and DMM. The intermediate FA is the key component in the reaction network observed.

Further investigations should focus on a refinement of the reaction kinetic model by applying different kinetic approaches considering elementary catalytic steps, which are already described by *Broomhead* et al. [43], e.g., applying mechanistic descriptions according to Christiansen [54,55]. Since radial effects caused by the distributed dosage of O_2 via the membrane are not considered in the simplified 1D model used for the simulation studies presented in this work, detailed 2D simulation studies should be performed in future work. Furthermore, a coupling between the momentum, mass, and heat balances should be considered to figure out hot spot effects on the scale-up of the reactor system from the laboratory into the pilot-plant level. Finally, validation experiments of the simulation results have to be done to prove the accuracy of the models used.

Author Contributions: Conceptualization, J.P.W. and C.H.; Methodology, J.P.W.; Software, J.P.W.; Validation, J.P.W.; Formal Analysis, J.P.W.; Investigation, J.P.W. and T.W.; Resources, T.W. and C.H.; Writing—Original Draft Preparation, J.P.W.; Writing—Review & Editing, T.W. and C.H.; Visualization, J.P.W.; Supervision, C.H.; Project Administration, C.H.; Funding Acquisition, C.H.; All authors have read and agreed to the published version of the manuscript.

Data Availability Statement: The data are available in the article.

Conflicts of Interest: The authors declare no conflict of interest.

Symbols

E_{ads,O_2}	$J \cdot mol^{-1}$	adsorption energy
E_A	$J \cdot mol^{-1}$	activation energy
J	$mol \cdot (m \cdot s)^{-1}$	molar flux
k	$mol \cdot kg^{-1} \cdot s^{-1} \cdot Pa^{-n}$	reaction rate constant
k_0	$mol \cdot kg^{-1} \cdot s^{-1} \cdot Pa^{-n}$	pre-exponential factor
K	Pa^{-1}	equilibrium constant of adsorption
K_0	Pa^{-1}	pre-exponential factor
K_{eq}	Pa^{-1}	equilibrium constant of reaction
L	m	reactor length
m_{cat}	kg	mass of catalyst
$\dot{n}$	$mol \cdot s^{-1}$	total molar flow rate
N_{exp}	-	number of experiments
p	Pa	pressure
r	$mol \cdot (kg \cdot s)^{-1}$	reaction rate
R	$J \cdot (mol \cdot K)^{-1}$	universal gas constant
S	-	selectivity
T	K	temperature
$\dot{V}$	$m^3 \cdot s^{-1}$	total volumetric flow rate
x	-	molar fraction
X	-	conversion
Y	-	yield
z	m	axial coordinate

Greek letters

ΔH_r	$J \cdot mol^{-1}$	enthalpy of reaction
ΔS_r	$J \cdot mol^{-1} \cdot K^{-1}$	entropy of reaction
λ	-	performance indicator (conversion, selectivity, yield)
ν	-	stoichiometric coefficient
Θ	-	Weisz-Prater criterion

Subscripts

exp	experimental
i	component index
in	inlet
j	reaction index
sim	simulated
ss	shell-side
ts	tube-side

Abbreviations

DMM	dimethoxymethane
eq.	equation
FBR	fixed-bed reactor
MeOH	methanol
MF	methyl formate
OF	objective function
O_2	oxygen
PBMR	packed-bed membrane reactor
ts/ss	tube-to-shell side feed ratio
WHSV	weight hourly space velocity

References

1. Ueckerdt, F.; Bauer, C.; Dirnaichner, A.; Everall, J.; Sacchi, R.; Luderer, G. Potential and risks of hydrogen-based e-fuels in climate change mitigation. *Nat. Clim. Chang.* **2021**, *11*, 384–393. [CrossRef]
2. Ehmann, K.R.; Nisters, A.; Vorholt, A.J.; Leitner, W. Carbon Dioxide Hydrogenation to Formic Acid with Self-Separating Product and Recyclable Catalyst Phase. *ChemCatChem* **2022**, *14*. [CrossRef]

3. Klemm, E.; Lobo, C.M.S.; Löwe, A.; Schallhart, V.; Renninger, S.; Waltersmann, L.; Costa, R.; Schulz, A.; Dietrich, R.-U.; Möltner, L.; et al. CHEMampere: Technologies for sustainable chemical production with renewable electricity and CO_2, N_2, O_2, and H_2O. *Can. J. Chem. Eng.* **2022**. [CrossRef]

4. Ott, J.; Gronemann, V.; Pontzen, F.; Fiedler, E.; Grossmann, G.; Kersebohm, D.B.; Weiss, G.; Witte, C. Methanol. In *Ullmann's Encyclopedia of Industrial Chemistry*; Wiley-VCH Verlag GmbH & Co. KGaA: Weinheim, Germany, 2000; ISBN 3527306730.

5. Bertau, M.; Räuchle, K.; Offermanns, H. Methanol—Die Basischemikalie. *Chem. Unserer Zeit* **2015**, *49*, 312–329. [CrossRef]

6. Oestreich, D.; Lautenschütz, L.; Arnold, U.; Sauer, J. Reaction kinetics and equilibrium parameters for the production of oxymethylene dimethyl ethers (OME) from methanol and formaldehyde. *Chem. Eng. Sci.* **2017**, *163*, 92–104. [CrossRef]

7. Hackbarth, K.; Haltenort, P.; Arnold, U.; Sauer, J. Recent Progress in the Production, Application and Evaluation of Oxymethylene Ethers. *Chem. Ing. Tech.* **2018**, *90*, 1520–1528. [CrossRef]

8. Zhao, Y.; Qin, Z.; Wang, G.; Dong, M.; Huang, L.; Wu, Z.; Fan, W.; Wang, J. Catalytic performance of V2O5/ZrO2–Al2O3 for methanol oxidation. *Fuel* **2013**, *104*, 22–27. [CrossRef]

9. Zhao, H.; Bennici, S.; Cai, J.; Shen, J.; Auroux, A. Influence of the metal oxide support on the surface and catalytic properties of sulfated vanadia catalysts for selective oxidation of methanol. *J. Catal.* **2010**, *274*, 259–272. [CrossRef]

10. Guo, H.; Chen, C.; Xiao, Y.; Wang, J.; Fan, Z.; Li, D.; Sun, Y. Influence of preparation method on the surface and catalytic properties of sulfated vanadia–titania catalysts for partial oxidation of methanol. *Fuel Process. Technol.* **2013**, *106*, 77–83. [CrossRef]

11. Liu, H.; Iglesia, E. Selective oxidation of methanol and ethanol on supported ruthenium oxide clusters at low temperatures. *J. Phys. Chem. B* **2005**, *109*, 2155–2163. [CrossRef]

12. Tatibouët, J.M. Methanol oxidation as a catalytic surface probe. *Appl. Catal. A Gen.* **1997**, *148*, 213–252. [CrossRef]

13. Thavornprasert, K.; Capron, M.; Jalowiecki-Duhamel, L.; Gardoll, O.; Trentesaux, M.; Mamede, A.-S.; Fang, G.; Faye, J.; Touati, N.; Vezin, H.; et al. Highly productive iron molybdate mixed oxides and their relevant catalytic properties for direct synthesis of 1,1-dimethoxymethane from methanol. *Appl. Catal. B Environ.* **2014**, *145*, 126–135. [CrossRef]

14. Thavornprasert, K.; Capron, M.; Jalowiecki-Duhamel, L.; Dumeignil, F. One-pot 1,1-dimethoxymethane synthesis from methanol: A promising pathway over bifunctional catalysts. *Catal. Sci. Technol.* **2016**, *6*, 958–970. [CrossRef]

15. Jacob, E. C-1 Oxygenate als nachhaltige Kraftstoffe und deren günstige Eigenschaften. In *Zukünftige Kraftstoffe*; Maus, W., Ed.; Springer: Berlin/Heidelberg, Germany, 2019; pp. 155–180. ISBN 978-3-662-58005-9.

16. Kaiser, D.; Beckmann, L.; Walter, J.; Bertau, M. Conversion of Green Methanol to Methyl Formate. *Catalysts* **2021**, *11*, 869. [CrossRef]

17. Benajes, J.; García, A.; Monsalve-Serrano, J.; Martínez-Boggio, S. Potential of using OMEx as substitute of diesel in the dual-fuel combustion mode to reduce the global CO2 emissions. *Transp. Eng.* **2020**, *1*, 100001. [CrossRef]

18. Martins, J.; Brito, F.P. Alternative Fuels for Internal Combustion Engines. *Energies* **2020**, *13*, 4086. [CrossRef]

19. Kaichev, V.V.; Popova, G.; Chesalov, Y.; Saraev, A.A.; Zemlyanov, D.Y.; Beloshapkin, S.A.; Knop-Gericke, A.; Schlögl, R.; Andrushkevich, T.V.; Bukhtiyarov, V.I. Selective oxidation of methanol to form dimethoxymethane and methyl formate over a monolayer V2O5/TiO2 catalyst. *J. Catal.* **2014**, *311*, 59–70. [CrossRef]

20. Burger, J.; Siegert, M.; Ströfer, E.; Hasse, H. Poly(oxymethylene) dimethyl ethers as components of tailored diesel fuel: Properties, synthesis and purification concepts. *Fuel* **2010**, *89*, 3315–3319. [CrossRef]

21. Maier, T.; Härtl, M.; Jacob, E.; Wachtmeister, G. Dimethyl carbonate (DMC) and Methyl Formate (MeFo): Emission characteristics of novel, clean and potentially CO2-neutral fuels including PMP and sub-23 nm nanoparticle-emission characteristics on a spark-ignition DI-engine. *Fuel* **2019**, *256*, 115925. [CrossRef]

22. Sun, J.; Li, H.; Song, H.; Wu, Q.; Zhao, Y.; Jiao, Q. Synthesis of methylal from methanol and formaldehyde catalyzed by Brønsted acid ionic liquids with different alkyl groups. *RSC Adv.* **2015**, *5*, 87200–87205. [CrossRef]

23. Baranowski, C.J.; Bahmanpour, A.M.; Kröcher, O. Catalytic synthesis of polyoxymethylene dimethyl ethers (OME): A review. *Appl. Catal. B Environ.* **2017**, *217*, 407–420. [CrossRef]

24. Bhatelia, T.; Lee, W.J.; Samanta, C.; Patel, J.; Bordoloi, A. Processes for the production of oxymethylene ethers: Promising synthetic diesel additives. *Asia-Pac. J. Chem. Eng.* **2017**, *12*, 827–837. [CrossRef]

25. Verfahren zur Herstellung von Methylformiat durch Umsetzung von Methanol mit Kohlenmonoxid in Gegenwart eines Katalysatorsystems, das Alkaliformiat und Alkalialkoholat Enthält—European Patent Office—EP 2922815 B1. Available online: https://patentimages.storage.googleapis.com/4b/4e/85/35f7d91d1e7989/EP0427062B1.pdf (accessed on 8 March 2023).

26. Rong, L.; Xu, Z.; Sun, J.; Guo, G. New methyl formate synthesis method: Coal to methyl formate. *J. Energy Chem.* **2018**, *27*, 238–242. [CrossRef]

27. Reutemann, W.; Kieczka, H. Formic Acid. In *Ullmann's Encyclopedia of Industrial Chemistry*; Wiley-VCH Verlag GmbH & Co. KGaA: Weinheim, Germany, 2000; ISBN 3527306730.

28. Lee, J.S.; Kim, J.C.; Kim, Y.G. Methyl formate as a new building block in C1 chemistry. *Appl. Catal.* **1990**, *57*, 1–30. [CrossRef]

29. Niethammer, B.; Wodarz, S.; Betz, M.; Haltenort, P.; Oestreich, D.; Hackbarth, K.; Arnold, U.; Otto, T.; Sauer, J. Alternative Liquid Fuels from Renewable Resources. *Chem. Ing. Tech.* **2018**, *90*, 99–112. [CrossRef]

30. Meng, Y.; Wang, T.; Chen, S.; Zhao, Y.; Ma, X.; Gong, J. Selective oxidation of methanol to dimethoxymethane on V2O5–MoO3/γ-Al2O3 catalysts. *Appl. Catal. B Environ.* **2014**, *160–161*, 161–172. [CrossRef]

31. Tatibouët, J.-M.; Lauron-Pernot, H. Transient isotopic study of methanol oxidation on unsupported V2O5. *J. Mol. Catal. A Chem.* **2001**, *171*, 205–216. [CrossRef]

32. Sun, Q.; Fu, Y.; Liu, J.; Auroux, A.; Shen, J. Structural, acidic and redox properties of V_2O_5-TiO_2-SO_4^{2-} catalysts. *Appl. Catal. A Gen.* **2008**, *334*, 26–34. [CrossRef]

33. Zhao, H.; Bennici, S.; Shen, J.; Auroux, A. Nature of surface sites of V_2O_5–TiO_2/SO_4^{2-} catalysts and reactivity in selective oxidation of methanol to dimethoxymethane. *J. Catal.* **2010**, *272*, 176–189. [CrossRef]

34. Chen, S.; Meng, Y.; Zhao, Y.; Ma, X.; Gong, J. Selective Oxidation of Methanol to Dimethoxymethane over Mesoporous Al-P-V-O Catalysts. *AIChE J.* **2013**, *59*, 2587–2593. [CrossRef]

35. Fan, Z.; Guo, H.; Fang, K.; Sun, Y. Efficient V_2O_5/TiO_2 composite catalysts for dimethoxymethane synthesis from methanol selective oxidation. *RSC Adv.* **2015**, *5*, 24795–24802. [CrossRef]

36. Chen, S.; Ma, X. The role of oxygen species in the selective oxidation of methanol to dimethoxymethane over VO_x/TS-1 catalyst. *J. Ind. Eng. Chem.* **2017**, *45*, 296–300. [CrossRef]

37. Tao, M.; Wang, H.; Bin Lu, B.L.; Zhao, J.; Cai, Q. Highly selective oxidation of methanol to dimethoxymethane over SO_4^{2-}/V_2O_5–ZrO_2. *New J. Chem.* **2017**, *41*, 8370–8376. [CrossRef]

38. Sun, R.; Delidovich, I.; Palkovits, R. Dimethoxymethane as a Cleaner Synthetic Fuel: Synthetic Methods, Catalysts, and Reaction Mechanism. *ACS Catal.* **2019**, *9*, 1298–1318. [CrossRef]

39. Kaichev, V.V.; Popova, G.Y.; Chesalov, Y.A.; Saraev, A.A.; Andrushkevich, T.V.; Bukhtiyarov, V.I. Active component of supported vanadium catalysts in the selective oxidation of methanol. *Kinet. Catal.* **2016**, *57*, 82–94. [CrossRef]

40. Gao, X.; Zhang, J.; Song, F.; Zhang, Q.; Han, Y.; Tan, Y. Selective oxidation conversion of methanol/dimethyl ether. *Chem. Commun.* **2022**, *58*, 4687–4699. [CrossRef]

41. Klose, F. *Structure-Activity Relations of Supported Vanadia Catalysts and the Potential of Membrane Reactors for the Oxidative Dehydrogenation of Ethane*, 1st ed.; Magdeburg, Univ., Fak. für Verfahrens- und Systemtechnik, Habil.-Schr.: Magdeburg, Germany, 2008; ISBN 978-3-939665-59-5.

42. Walter, J.P. Selective Oxidation of Methanol to Green Oxygenates—Feasibility Study of Fixed-Bed and Membrane Reactors. *Chem. Ing. Tech.* **2023**. [CrossRef]

43. Broomhead, W.T.; Tian, W.; Herrera, J.E.; Chin, Y.-H.C. Kinetic Coupling of Redox and Acid Chemistry in Methanol Partial Oxidation on Vanadium Oxide Catalysts. *ACS Catal.* **2022**, *12*, 11801–11820. [CrossRef]

44. Deshmukh, S.; van Annaland, M.S.; Kuipers, J. Kinetics of the partial oxidation of methanol over a Fe-Mo catalyst. *Appl. Catal. A Gen.* **2005**, *289*, 240–255. [CrossRef]

45. Kapteijn, F.; van de Graaf, J.M.; Moulijn, J.A. One-component permeation maximum: Diagnostic tool for silicalite-1 membranes? *AIChE J.* **2000**, *46*, 1096–1100. [CrossRef]

46. Yaws, C.L. *The Yaws Handbook of Thermodynamic Properties for Hydrocarbons and Chemicals*; Gulf: Houston, TX, USA, 2006; ISBN 1933762071.

47. Ościk, J. *Adsorption*; Horwood, E., Ed.; Halsted Press: Chichester, NY, USA, 1982; ISBN 83-01-02568-9.

48. Emig, G.; Klemm, E. *Chemische Reaktionstechnik*, 6th ed.; Springer Vieweg: Berlin/Heidelberg, Germany, 2017; ISBN 978-3-662-49267-3.

49. Hamel, C.; Tóta, Á.; Klose, F.; Tsotsas, E.; Seidel-Morgenstern, A. Analysis of single and multi-stage membrane reactors for the oxidation of short-chain alkanes—Simulation study and pilot scale experiments. *Chem. Eng. Res. Des.* **2008**, *86*, 753–764. [CrossRef]

50. Walter, J.P.; Brune, A.; Seidel-Morgenstern, A.; Hamel, C. Model-based Analysis of Fixed-bed and Membrane Reactors of Various Scale. *Chem. Ing. Tech.* **2021**, *93*, 819–824. [CrossRef]

51. Walter, J.P.; Brune, A.; Seidel-Morgenstern, A.; Hamel, C. Process Intensification of the Propane Dehydrogenation Considering Coke Formation, Catalyst Deactivation and Regeneration—Transient Modelling and Analysis of a Heat-Integrated Membrane Reactor. *Catalysts* **2021**, *11*, 1056. [CrossRef]

52. Brune, A.; Wolff, T.; Seidel-Morgenstern, A.; Hamel, C. Analysis of Membrane Reactors for Integrated Coupling of Oxidative and Thermal Dehydrogenation of Propane. *Chem. Ing. Tech.* **2019**, *91*, 645–650. [CrossRef]

53. Hamel, C.; Seidel-Morgenstern, A. Potenzial von Membranen zur verbesserten Reaktionsführung von Selektivoxidationen: Katalysator-, Reaktor- und Prozessebene. *Chem. Ing. Tech.* **2022**, *94*, 56–69. [CrossRef]

54. Christiansen, J.A. *The Elucidation of Reaction Mechanisms by the Method of Intermediates in Quasi-Stationary Concentrations*; Elsevier: Amsterdam, The Netherlands, 1953; pp. 311–353. ISBN 9780120078059.

55. Helfferich, F.G. *Kinetics of Multistep Reactions (Comprehensive Chemical Kinetics, 0069-8040; v. 40)*; Elsevier Science Limited: Amsterdam, The Netherlands, 2004; ISBN 9780080473185.